The rôle of grain diameter in dune dynamics

Alexandros A. Rispo Constantinou
Supervised by Karol A. Bacik and D^r. Nathalie M. Vriend.

MMXIX

Abstract

Expressions exist in the literature for the sediment flux above a bed of grains in terms of the grains' diameter and the velocity of the surrounding fluid [4, p. 268; 1, p. 335]. These generally neglect the effects of cohesion between the grains and the bed: by adapting the derivation of Andreotti, Forterre & Pouliquen [1, p. 324] for the threshold fluid velocity for particle entrainment, we obtain a cohesive expression for the sediment flux. The migration rate of quasi-two-dimensional dunes is measured experimentally and found to substantiate existing theories. These are compared to a cohesive model, which proves to match the data more closely, although due to inadequate data this result is inconclusive — albeit suggestive.

I · INTRODUCTION

Dunes are a naturally occurring phenomenon wherever the motion of a granular sediment is dictated by the flow of an ambient fluid. They range in size from the small subaqueous ripple marks found in the shallows of beaches to the large roaming dunes of the Curonian spit, which have been known to bury the occasional village. Able to form under the influence of the wind just as well as under that of water currents, dunes form a rich typology, from the characteristically crescent-shaped barchan dune, to the largely two-dimensional contour of transverse dunes, to even more complex structures such as the poetically-named star dune [20; 18].

Sediment transport in dunes has been a topic of active study since the mid-thirties [19]; researchers seek for example to quantify how dunes develop, how they interact and, notably, how they locomote. But sand varies from desert to desert, and it is still not clear how these behaviours depend on the exact properties of the sediment composing the dunes.

For this project, we have chosen to study the migration rate of a dune in a narrow channel, and its dependence on the size of its constituent grains. Such quasi-two-dimensional dunes model large transverse-dune fields, or the central cross-section of a crescent-shaped barchan dune. By collecting data on dunes of a number of sizes and monodisperse granular compositions, subjec-

ted to increasingly rapid flows, we substantiate a more general, cohesive theoretical prediction for the dependence of the migration rate of the dune on the diameter of its grains.

II · THEORETICAL PREDICTIONS

Two-dimensional dunes will have some topography $h(x,t)$ in a static frame of reference. Sediment moves over this topography from the tail to the crest of the dune, and subsequently avalanches over the lee slope; we locally quantify this movement by the particle mass flux $q(x,t)$ $[\frac{\mathrm{kg}}{\mathrm{m\,s}}]$. Writing down the equation for mass conservation of the dune yields the Exner equation [10]:

$$\varrho_\mathrm{g}\phi\,\frac{\partial h}{\partial t}+\frac{\partial q}{\partial x}=0. \tag{1}$$

A neat trick [5] now consists in transforming to a coördinate frame comobile with the dune ($x'=x-ct, t'=t$); then, assuming time-similarity of the topography in this new frame ($\partial h/\partial t'=0$), we obtain a modified equation

$$\frac{\partial q}{\partial x'}=\varrho_\mathrm{g}\phi c\,\frac{\partial h}{\partial x'}.$$

This expression can be integrated to give the rule

$$c=\frac{\mathrm{Q}-\varrho}{\varrho_\mathrm{g}\phi\mathrm{H}}, \tag{2}$$

where $\mathrm{H}=h(\text{crest})$ is the height of the dune, $\mathrm{Q}=q(\text{crest})$ the sediment flux across the crest and $\varrho=q(\text{tail})$ the influx at the tail. This last quantity we assume to be negligible compared to Q (on the order of a few grains a second).

If we further assume the mobile layer to consist of grains of uniform diameter d moving at a uniform speed u_g, we can split the saturated mass flux into a particle flux n $[\mathrm{m}^{-2}]$ and a grain velocity u_g — that is to say,

$$q_\mathrm{sat}\simeq\frac{\pi}{6}\varrho_\mathrm{g}\,d^3\cdot n\cdot u_\mathrm{g}, \tag{3}$$

— and individually address these two terms.

Grain speed. — The grain speed is governed by a balance between the propulsive (drag) and resistive (friction) forces. We suggest that the cohesive property of the granular medium, whilst weak, is sufficient to have a visible effect on the migration rate; we hence set our force balance to be

$$\mu_\mathrm{k}\,\mathrm{F}_\mathrm{weight}+\mu_\mathrm{k}\,\mathrm{F}_\mathrm{cohesion}=\mathrm{F}_\mathrm{drag}. \tag{4}$$

For the cohesive force, we postulate an expression of the form $\mathrm{F}\simeq\pi\gamma_\mathrm{eff}d$.* Substituting this expression into (4) along with expressions for the drag and weight, we obtain

$$\frac{\pi}{6}\mu_\mathrm{k}\big(\varrho_\mathrm{g}-\varrho_\mathrm{f}\big)gd^3+\mu_\mathrm{k}\pi\gamma_\mathrm{eff}d \simeq\frac{\pi}{16}\mathrm{C}_\infty\varrho_\mathrm{f}\big(u_*-u_\mathrm{g}\big)^2d^2, \tag{5}$$

where we denote u_* the turbulent shear velocity of the fluid flow. Note that when the fluid is at the threshold velocity $u_{*\mathrm{th}}$, the grain velocity must be zero (and the friction coëfficient static); substituting these values and rearranging leads to an expression for the threshold velocity of

$$u_{*\mathrm{th}}\simeq\sqrt{\frac{8\mu_\mathrm{s}}{3\mathrm{C}_\infty}\left(\left(\frac{\varrho_\mathrm{g}}{\varrho_\mathrm{f}}-1\right)gd+\frac{6\gamma_\mathrm{eff}}{d}\right)}.$$

*The van der Waals force between a sphere and a wall in contact is $\mathrm{F}_\mathrm{vdW}\simeq\mathrm{H}d/6z_0^2$ where z_0 is the (intermolecular) surface-to-surface separation and H the Hamaker constant [15]. The linear dependence of the cohesive force on d can alternatively be derived as a difference in surface tension following from variations in contact area of the grains during displacements [1, § 2.2.2].

This can be rephrased in terms of a cohesive length scale

$$d_\gamma := \sqrt{\frac{6\gamma_{\text{eff}}}{(\varrho_g - \varrho_f)g}} \qquad \text{as} \tag{6}$$

$$u_{*\text{th}} \simeq \sqrt{\frac{8\mu_s}{3C_\infty}\left(\frac{\varrho_g}{\varrho_f} - 1\right) gd\left(1 + \left(\frac{d_\gamma}{d}\right)^2\right)}. \tag{7}$$

Since in (5) the left-hand side is constant for any fluid velocity $u_* > u_{*\text{th}}$ the right-hand side cannot have any dependence on it, and we must conclude that the right-hand side is a constant multiple of the square of the threshold velocity:

$$\begin{aligned} \left(u_* - u_g\right)^2 &= \mu_k \cdot \frac{1}{\mu_s} u_{*\text{th}}^2 \\ \implies u_g &= u_* - \sqrt{\frac{\mu_k}{\mu_s}}\, u_{*\text{th}}. \end{aligned} \tag{8}$$

We denote by υ the quantity $\sqrt{\frac{\mu_k}{\mu_s}}$.[‡]

Particle flux. — This is difficult to calculate, and derivations are largely heuristic. One traditional argument is the so-called transporting machine by Bagnold [4; 3], in which the mobile layer is a moving carpet lubricating the immobile layer. We instead choose to use the derivation by Andreotti, Forterre & Pouliquen [1], which models a single mobile layer subjected to a stress τ from the ambient fluid; this layer then exerts a stress τ_b on the immobile layer below it. The resulting stress balance is

$$\tau_b = \tau - n \cdot \mu_k \left(F_{\text{weight}} + F_{\text{cohesion}}\right). \tag{9}$$

It is claimed [1, p. 334] that equilibrium is reached when the bottom layer is at the transport threshold, *i. e.* $\tau_b = \tau_{\text{th}}$. Using the heuristic that $\tau \simeq \varrho_f u^2$, we can rearrange to find an expression for n in terms of u_* and $u_{*\text{th}}$, into which we can substitute the same forces as in (5) to obtain

$$n = \frac{6/\pi}{\mu_k d^2}\left(1 + \left(\frac{d_\gamma}{d}\right)^2\right)^{-1} \frac{u_*^2 - u_{*\text{th}}^2}{\left(\frac{\varrho_g}{\varrho_f} - 1\right)gd}. \tag{10}$$

Saturated flux. — We can combine our newfound expressions for the grain velocity (8) and for the particle flux (10) with (3) to obtain an expression for the saturated flux

$$q_{\text{sat}} \simeq \frac{\varrho_g}{\mu_k} \frac{\left(u_* - \upsilon u_{*\text{th}}\right)\left(u_*^2 - u_{*\text{th}}^2\right)}{\left(1 + \left(\frac{d_\gamma}{d}\right)^2\right)\left(\frac{\varrho_g}{\varrho_f} - 1\right)g}. \tag{11}$$

This is now ripe for inclusion in (2) to yield a prediction for a dune's migration rate:

$$c \simeq \frac{1}{\mu_k \phi H} \frac{\left(u_* - \upsilon u_{*\text{th}}\right)\left(u_*^2 - u_{*\text{th}}^2\right)}{\left(1 + \left(\frac{d_\gamma}{d}\right)^2\right)\left(\frac{\varrho_g}{\varrho_f} - 1\right)g}, \tag{12}$$

in which spatially-dependent quantities are evaluated at the crest and the influx ϱ is neglected.

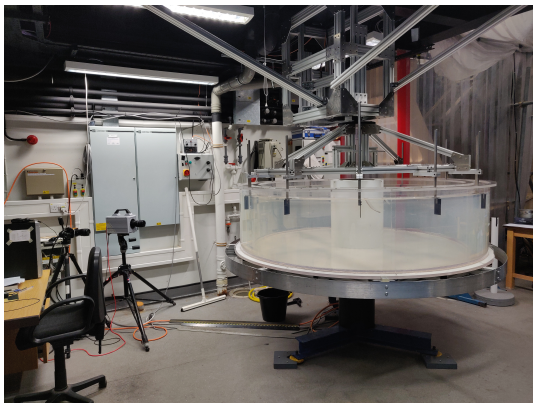

Figure 1: The apparatus (tank, spider, cameras).

[‡] Allowing for $\upsilon \neq 1$ in this derivation resolves a technicality regarding the threshold, as experimental evidence suggests that the grain velocity *does not* vanish at the threshold, unlike the grain flux n [8; 1, p. 334]. (*N. b.* — in [1], $\Upsilon = \upsilon^2$.)

III · EXPERIMENTAL APPARATUS

A photograph of the experimental apparatus is presented in fig. 1. An open annular flume or tank of external radius 97 cm, width 9 cm and depth approximately 50 cm rotates on a powered turntable. Above the tank rests a frame, called the s p i d e r, which holds twelve 8 cm × 10 cm paddles of adjustable height — fixed, in this experiment, at *c.* 34 cm above the floor of the tank.[**] Both assemblies are controlled independently and are counter-rotated to generate a flow within the flume, minimising the effect of fictitious forces.

The flume was filled with water to a depth of approximately 1 cm above the top of the paddles, and a heap of either 1, 1.5 or 2 litres of granular material was placed into the tank in such a way as to form a symmetrical heap at the angle of repose. The material consisted of soda-glass ballotini of specific gravity nominally 2.55 kg/l, which we verified experimentally to be correct within approximately one part in twenty.[†] Four diameters were used, marked by the supplier as $d_1 = 0.4$–0.6 mm, $d_2 = 1.0$ mm, $d_3 = 2.0$ mm and $d_4 = 3.1$ mm. These were not independently verified.[‡] The set-up was spun at four total rotation rates Ω between 11.0 and 15.5 rpm, maintaining a ratio of approximately -1.35 between the rotation of the table and that of the spider (table 1). We performed in total forty-eight experimental runs.

The experiment was started from rest and ran continuously for 25 min. Data were captured from two fixed cameras: one provided uninterrupted footage of the experiment at 200 fps, and was used to obtain the height of the granular bed-form in the flume, accurate to individual millimetres; the other camera took twelve 2000 fps-snapshots of the bed-form at intervals of approximately two minutes, providing data for the velocimetry. For every snapshot we took an average of the horizontal component of the velocity in a region of about 5.5 cm in height beginning 1 cm above the back of the dune, using the methodology developed by Bacik et al. [2]. We then took an average of this quantity over the last eleven snapshots to obtain our analogue v for the turbulent shear velocity u_*. We expect this quantity to be a constant multiple of the turbulent shear velocity and will use it exclusively in our treatment of the experimental data as a proxy for u_*.[§]

Ω	Ω_{spider}	$-\Omega_{\text{table}}$	$\left\lvert\frac{\Omega_{\text{spider}}}{\Omega_{\text{table}}}\right\rvert$
11.0	6.3	4.7	1.34
12.5	7.2	5.3	1.36
14.0	8.1	5.9	1.37
15.5	8.9	6.6	1.35

Table 1: Rotation rate decomposition [rpm].

IV · RESULTS

The footage from the continuous capture was split into an integer number of data sets, referred

[**] *For Karol: this has the rods jutting 26 cm above the spider.*

[†] This we achieved by exploiting the change in weight of a graduated cylinder initially filled with grains to which we subsequently added water to a known volume.

[‡] A more detailed description may be available soon, a sample of the particles having been sent for analysis.

[§] Assuming above the bed a logarithmic velocity profile $u(y) = \frac{u_*}{\varkappa}\log\left(\frac{y}{д}\right)$ uniform along the flume (where $\varkappa$ is von Kármán's constant and $д$ the surface roughness) [7], the conversion rule is

$$v = \langle u\rangle = \frac{1}{b-a}\int_a^b u = u_* \cdot \left[\frac{д/\varkappa}{(b-a)}\int_{a/д}^{b/д}\log\right],$$

for appropriate bounds a and b.

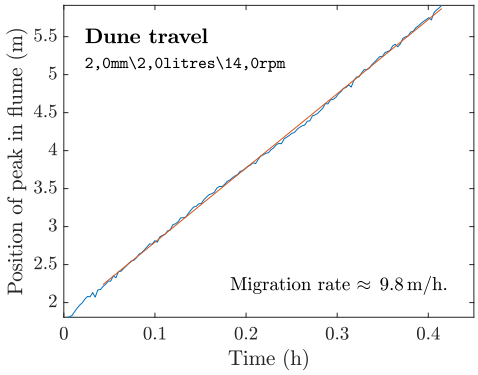

Figure 2: An example plot whence is calculated the migration rate.

to as profiles, corresponding to individual tank rotations with a branch cut provided by a distinguished point on the table. From these we can extract the height of the sediment at discretised intervals along the flume to generate space-time diagrams such as that in the appendix (fig. 14, p. xvii). The position of the highest point of the sediment is then tracked to provide a reference position for the dune; plotting this, we obtain summaries of the dune's motion (fig. 2; also figs. 15 and 16). We note that after an initial shape transition the dune progresses at a constant rate: an affine fit is appropriate. To optimise the accuracy of the fit, we wish to choose a point at which to begin fitting that is in the steady state for all experimental runs; to that end, we can track locally two quantities we expect to be stable in the steady state, and verify that they settle to a constant value. Figures 3 and 4 show this stabilisation; we choose to begin fitting at profile number 20.

We can read off the gradient of the affinely fitted position to provide the migration speed of the dune along the flume for that run. The dune height H is averaged over all heights measured throughout the experimental run, once judged to

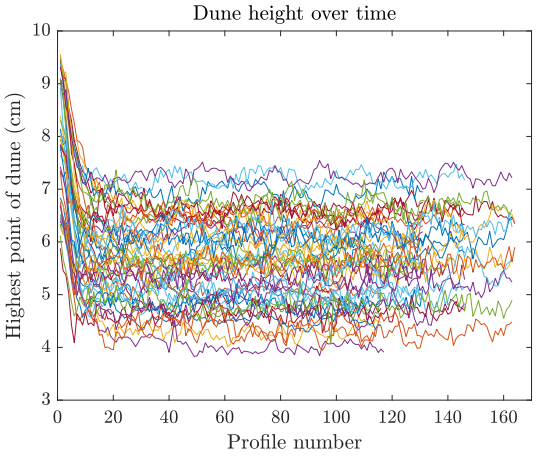

Figure 3: Dune height over time, plotted for all the experimental runs. *The height always appears to have settled by profile n^o 20.*

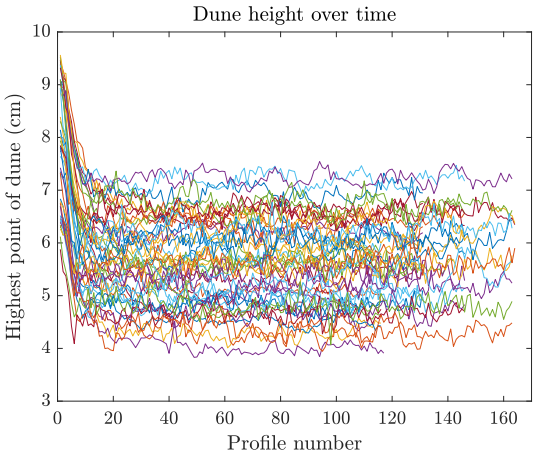

Figure 4: Local dune speed over time, plotted for all the experimental runs. *This is calculated through a method of differences.*

d	$k_1/10^3$	k_2
d_1	1.032	0.405
d_2	1.571	0.448
d_3	1.921	0.569
d_4	2.476	0.585

Table 2: Values for k_1 and $k_2 = v_{\text{th}}$. *We have fixed the friction ratio* $\upsilon^2 = 0.4976$.

be in the steady state by the aforementioned criterion. To verify the expression for c given in (12), we require the knowledge of three quantities: υ, d_γ and $u_{*\text{th}}$. These will be left as free parameters in our fits. The former two are expected to be constant throughout the experiments, whereas the last is expected to depend on d (*v.* (7)). Reference values suggest $\upsilon^2 = \mu_k/\mu_s \approx 1/2$ [14]. To verify this, we plot cH against the fluid velocity v obtained from the velocimetry; we then use the MATLAB routine `lsqcurvefit` to fit a model of the form

$$\widehat{c\mathrm{H}} = k_1 \left(v/k_2 - k_3\right)\left(v^2 - k_3^2\right)$$

to every set of particle diameters (fig. 5). The coëfficients represent the quantities as

$$k_1 = \left(\mu_k \phi g \upsilon \left(1 + \left(\frac{d_\gamma}{d}\right)^2\right)\left(\frac{\varrho_g}{\varrho_f} - 1\right)\right)^{-1},$$

$$k_2 = \upsilon \quad \text{and} \quad k_3 = v_{\text{th}}.$$

The fit yields four values of k_3^2 for the four diameters d_1–d_4, of about 0.4928, 0.4947, 0.5012 and 0.5016 respectively. Hence we now run the analysis again with k_3^2 fixed at the mean of these values, or approximately 0.4976. We obtain the fits depicted in fig. 6, whose parameters are those given in table 2. This gives our estimates for the v_{th}.

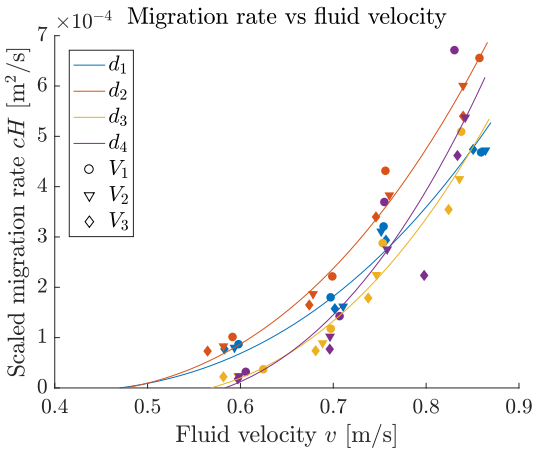

Figure 5: Three-parameter fitting.

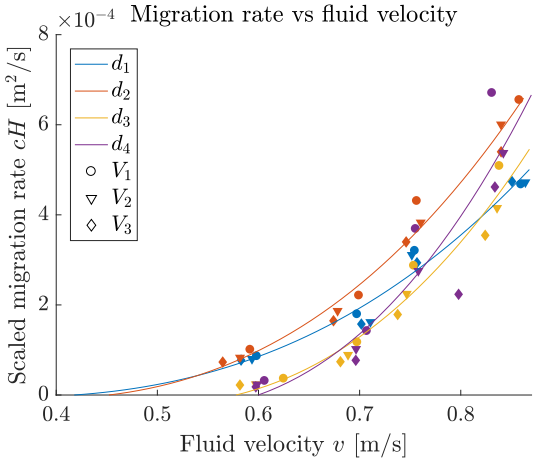

Figure 6: Two-parameter fitting $\left(\upsilon^2 = 0.4976\right)$. *From this we extract the intercepts for* v_{th}.

We have decided, for better or for worse, to keep d_γ as a free parameter (as recommended in [1]). This we estimate from the relatively simpler prediction (7) we have for the threshold shear velocity

$$u_{*\mathrm{th}} \propto \sqrt{d\left(1+\left(\frac{d_\gamma}{d}\right)^2\right)}, \qquad (13)$$

since this expression is on more solid theoretical ground than that for the particle flux n. The data we have at our disposal for this plot are, however, woefully inadequate: we must content ourselves with four points, which are themselves calculated by fitting. Ideally, we would have experimental data available for a wider range of particle sizes, with particularly fine resolution around the expected minimum, — or even an entirely different method, empirical or theoretical, — to obtain d_γ. However, things being as they are, we must continue regardless.

To utilise (13), we plot our estimates for v_{th} against d,[¶] to which we fit a curve

$$\widehat{v_{\mathrm{th}}} = l_1\sqrt{d\left(1+\left(\frac{l_2}{d}\right)^2\right)}$$

— a curve reassuringly similar to that reported empirically in [5]. For reference, fig. 7 also includes a fit with l_2 fixed at zero (incohesive case). From the cohesive fit, we obtain a value $d_\gamma \approx 0.7\,\mathrm{mm}$.

Thus armed, we are in a position to begin verifying the predictions of (12), which we recast as

$$c\mathrm{H}v_{\mathrm{th}}^{-3}\left(1+\left(\frac{d_\gamma}{d}\right)^2\right) \propto \left(\frac{v}{v_{\mathrm{th}}}-\upsilon\right)\left(\frac{v^2}{v_{\mathrm{th}}^2}-1\right).$$

[¶] The plots use $[d_1\ d_2\ d_3\ d_4] = [0.5\ 1.0\ 2.0\ 3.1]$. These numbers may be refined with a detailed analysis of the grain distributions.

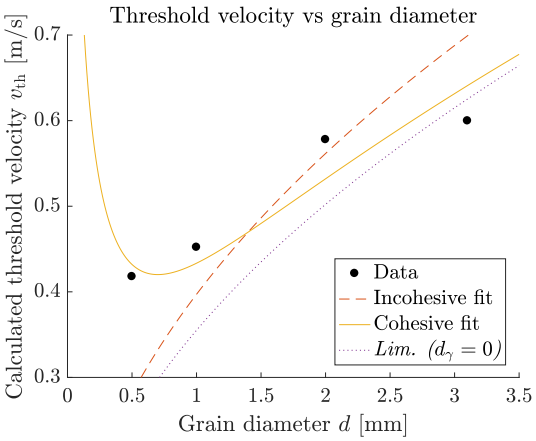

Figure 7: Threshold velocity in terms of particle diameter. *This plot is used to obtain an estimate for* d_γ. *Shown on the plot are* (i) *a fit for an incohesive prediction* ($l_2 \equiv 0$), (ii) *the full cohesive fit and* (iii) *the large-diameter limit for* (ii). *Note that* (i) *is the best fit of type* $\widehat{v_{th}} = l_1\, d^{1/2}$, *whereas* (iii) *merely uses the same* l_1*-value as* (ii).

We hope to obtain a linear relationship between the left-hand side and the right, which we plot in fig. 8. A logarithmic version of the same relationship is depicted in fig. 9. These two plots are to be contrasted with their corresponding incohesive versions, which have d_γ set to nought (figs. 10 and 11).

We see the data form a reasonably straight line, as predicted, and in fact the cohesive plot better fits the theoretical prediction than does the plot which ignores cohesion ($\mathrm{R}^2 = 0.9578$ *vs* $\mathrm{R}^2 = 0.8491$). Our cohesive fit is less accurate for smaller values of the grain diameter; this is only to be expected, since diameters near the critical diameter d_γ are more sensitive to error in d_γ. Despite the possibility that our extracted value for d_γ not be better than an order-of-magnitude estimate, the fact that the fit is best with the correction is a promising indicator of the need for a cohesive term.

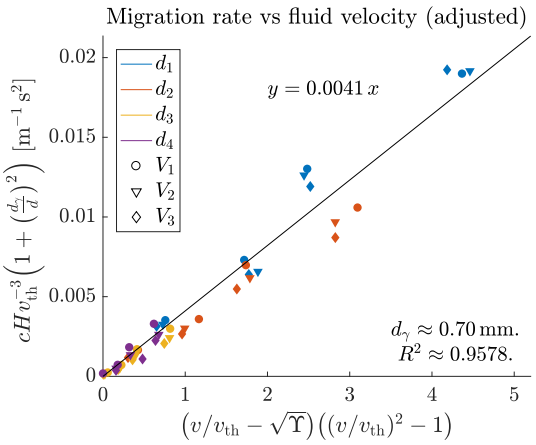

Figure 8: A candidate master curve. *Superposed is also the gradient of best fit.*

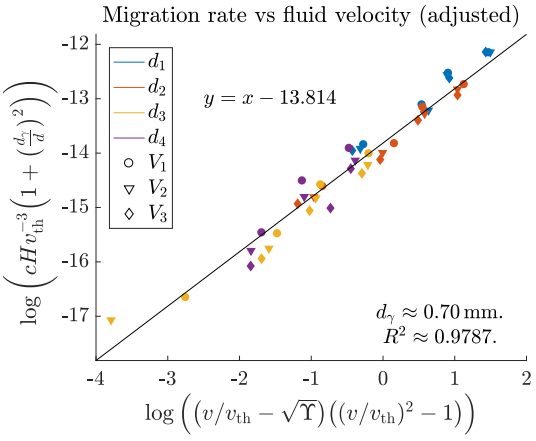

Figure 9: The candidate master curve, plotted logarithmically. *Overlain is the best-fitting affine line of gradient one.*

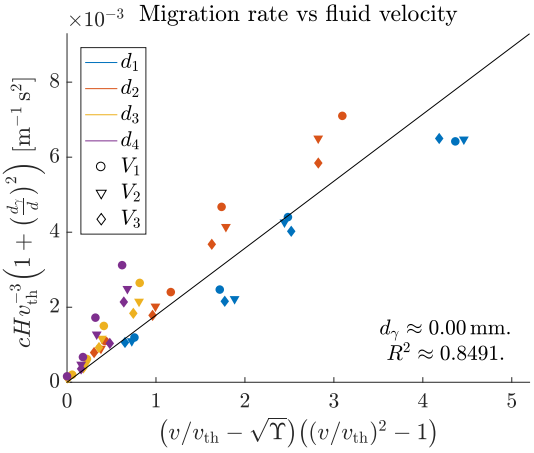

Figure 10: An incohesive version of fig. 8.

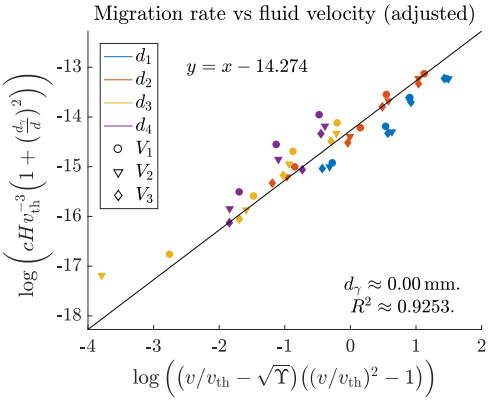

Figure 11: An incohesive version of fig. 9.

IV.1 Criticism

Of the data. — A number of parameters are obtained by fitting to data. Whereas one of these (υ) closely matches the theoretical prediction and is regularised by drawing on four sets of data, two others are of fickler standing. Every threshold velocity v_{th} is obtained from twelve data points; the value for d_γ, from only four. The correction term

$$\left(1+\left(\frac{d_\gamma}{d}\right)^2\right)$$

is quite sensitive to which side of unity the ratio d_γ/d lies, and as such our data cannot hope to adequately illustrate the predicted relationship between the desired quantities. It would be preferable to measure v_{th} independently — using an experiment better tailored to it, over a greater range of judiciously chosen particle diameters — and utilise those values to calculate the cohesive length scale d_γ and thence validate the theoretical prediction for our data. Despite these shortcomings, we find visible agreement with our prediction for particles sufficiently high above the characteristic length of cohesion.

Of the theory. — Perhaps the least satisfactory component of our derivation for c is in the treatment of n. Beyond its reliance on shear stresses, the derivation is flawed in that it assumes the presence of a single layer of mobile grains. This is not borne out experimentally: at faster rates of rotation, our dunes appeared to have in motion a layer of up to three times the grain diameter. Indeed, it is difficult to speak of individual layers moving, and a theory of n would have reconcile the continuum of the layer with the discrete nature of the moving grains. We furthermore expect the grains, which are almost stationary in the immobile layer and reach a maximum at the surface of the bed-form, to exhibit a profile of grain velocities u_g, and a more sophisticated theory would account for this as well [13].

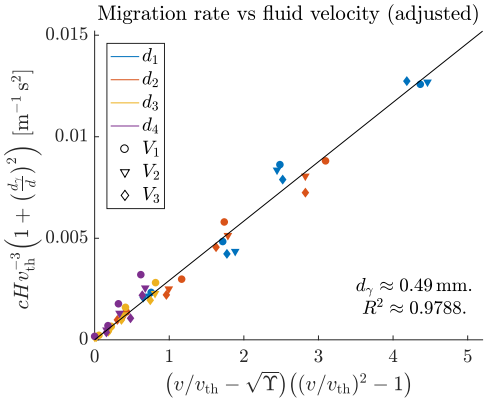

Figure 12: Another candidate for a master curve (*c.f.* fig. 8). *The parameter d_γ has been adjusted to provide the best possible* R^2 *with a resolution of ten microns.*

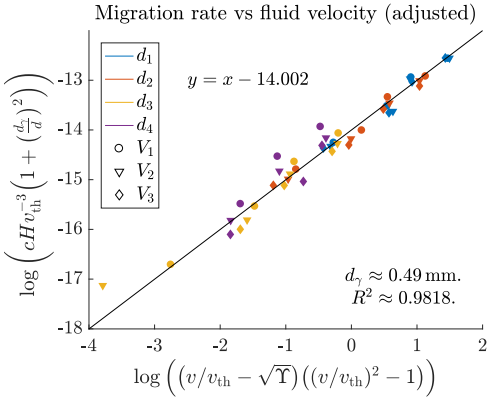

Figure 13: The logarithmic plot corresponding to fig. 12.

V · ADDENDA

V.1 Alternative for d_γ

If instead of attempting to extract d_γ from the threshold-velocity data, we look at which value of d_γ between 0.01 and 1 mm (in increments of 0.01 mm) produces the best fit for

$$cHv_{\text{th}}^{-3}\left(1+\left(\frac{d_\gamma}{d}\right)^2\right) \propto \left(\frac{v}{v_{\text{th}}}-\upsilon\right)\left(\frac{v^2}{v_{\text{th}}^2}-1\right)$$

in terms of R^2-value, we find $d_\gamma \approx 0.49\,\text{mm}$ (plotted in figs. 12 and 13). This is of the same order as our original prediction of $d_\gamma \approx 0.70\,\text{mm}$.

v.2 Nondimensionalisation

The Shields number is defined to be a nondimensional shear stress [1]

$$\Theta := \frac{\tau}{(\varrho_\mathrm{g} - \varrho_\mathrm{f})gd}. \tag{14}$$

If we postulate a velocity-dependent shear stress $\tau \simeq \varrho_\mathrm{f} u_*^2$, we obtain a conversion from our fluid velocity to the Shields number,

$$\Theta = \frac{u_*^2}{\left(\frac{\varrho_\mathrm{g}}{\varrho_\mathrm{f}} - 1\right)gd}. \tag{15}$$

Then we can partly nondimensionalise (12) to

$$c\mathrm{H} \simeq \frac{d}{\mu_\mathrm{k}\phi}\sqrt{\left(\frac{\varrho_\mathrm{g}}{\varrho_\mathrm{f}} - 1\right)gd}\Big/\left(1 + \left(\frac{d_\gamma}{d}\right)^2\right) \cdot \left(\sqrt{\Theta} - \upsilon\sqrt{\Theta}_\mathrm{th}\right)\cdot(\Theta - \Theta_\mathrm{th}).$$

If we further relabel $\mathfrak{H} := \mathrm{H}/d$ the height of the dune in grain diameters, $\mathfrak{G} := \left(d\big/d_\gamma\right)^{3/2}$ a nondimensional cohesive effect,[w] and

$$\mathfrak{C} := \frac{c}{\sqrt{\left(\frac{\varrho_\mathrm{g}}{\varrho_\mathrm{f}} - 1\right)gd}}$$

a nondimensional bed-form migration rate, we obtain the following nondimensional relationship:

$$\mathfrak{C} \simeq \frac{\left(\sqrt{\Theta} - \upsilon\sqrt{\Theta}_\mathrm{th}\right)\cdot(\Theta - \Theta_\mathrm{th})}{\mu_\mathrm{k}\phi\,\mathfrak{H}\left(1 + \mathfrak{G}^{-4/3}\right)}. \tag{16}$$

[w] By analogy with the Galilei number

$$\mathrm{Ga} := \left(\frac{d}{d_\nu}\right)^{3/2} = \sqrt{\left(\frac{\varrho_\mathrm{g}}{\varrho_\mathrm{f}} - 1\right)gd^3\Big/\nu^2}$$

as defined in [17], where

$$d_\nu := \sqrt[3]{\frac{\nu^2}{\left(\frac{\varrho_\mathrm{g}}{\varrho_\mathrm{f}} - 1\right)g}}$$

is a characteristic viscous diameter [1].

We can also reformulate (7) nondimensionally to give a threshold Shields number

$$\Theta_\mathrm{th} = \frac{8\mu_\mathrm{s}}{3\mathrm{C}_\infty}\left(1 + \mathfrak{G}^{-4/3}\right) \tag{17}$$

which agrees with the expression in [1].

v.3 Extensions

There are a number of improvements available, which have been abandoned due to constraints on the extent of the project. These include:

(i) *An error analysis on the data.* — We have reasonable estimates on the errors of all our quantities: it should merely be a matter of carrying them through.

(ii) *Consistency checks on the experimental runs.* — It is advisable to verify reproducibility of our data on the migration rate by picking one experiment and running it perhaps five more times to see that the dune settles into the same steady state.

(iii) *Robust dune tracking.* — To obtain the position of a dune, we have tracked its highest point. This measurement is sensitive to variations on the order of individual grains, and hence in some experiments is seen to oscillate irregularly with amplitude on the order of five centimetres. A more robust measure would be to compute the centre of mass of the dune by integrating $\int xh(x)\,\mathrm{d}x$ numerically. A similar procedure would allow an independent estimate of the dune's volume, though this is liable to fail under spanwise asymmetry.

(iv) *Sanity checks on coëfficients.* — In the course of our fits, we obtain a number of prefactors (figs. 8 and 9) which are predicted in the

theory in terms of ϕ, μ_k, ϱ_g/ϱ_f, *etc*. These can be compared to the fitted prefactors to establish whether they correspond to the theory (if only in order of magnitude).

(v) *Literature review on* υ. — The values on we based our initial estimate of υ are reference values for dry flat surfaces of glass in contact. Are these numbers appropriate for hydraulically lubricated spheres? It is not clear that this is the case.

(vi) *Particle influx.* — We have assumed that the influx of particles ϱ at the tail is negligible. This could be quantified using footage we already have from the velocimetric camera.

(vii) *Slope effects.* — Throughout our derivation, we assume that the grains lie on a flat horizontal bed. This assumption is justified by the fact that we only ever evaluate the saturated sediment flux q_{sat} at the crest of the dune, which is no more than a handful of degrees off the horizontal. However, a more detailed model might consider the presence of a more marked slope at the dune's tail.

(viii) Data by Julien [16], Fernandez Luque & Beek [11] (as reported in [1, fig. 8.9]) show agreement with the model

$$\log\left(\frac{q_{sat}}{\sqrt{\left(\frac{\varrho_g}{\varrho_f}-1\right)gd^3}}\right) \propto \log(\Theta - \Theta_{th}).$$

It would be interesting to reëvaluate their data (if available) in the light of our analysis and explore the data's agreement with our model.

v.4 Recommendations

A subsequent project might choose to draw on tributaries of this one. To that end, here is a list of suggested areas of enquiry:

(i) In our expression for the migration rate c, we have a term entirely unaccounted for: the packing fraction ϕ. We have assumed that this remains constant. It might be of interest to explore how the density of the dune as a system varies with various parameters, and thus establish the status of ϕ.

(ii) A significant drawback in our experiments has proved to be our inability to compute a good estimate for the cohesive length scale d_γ. It would benefit the theory greatly to investigate the exact value of this length scale in subaqueous bed-forms, either by performing the same experiments with a greater range of diameters in the range 0.1–1 mm or by developing a new method entirely (perhaps by looking at the angle of repose).

(iii) Finally, we have assumed for our derivation an entirely turbulent regime, which holds as a first approximation: we operate at a characteristic viscous length scale

$$d_\nu := \sqrt[3]{\frac{\nu^2}{\left(\frac{\varrho_g}{\varrho_f}-1\right)g}} \approx \sqrt[3]{\frac{10^{-12}}{1\cdot 10}} \approx 50\,\mu\text{m},$$

and at an approximate particle Reynolds number of

$$\text{Re} := \frac{u_* d}{\nu} \sim \frac{10^{-1}\cdot 10^{-3}}{10^{-6}} = 100$$

(order of magnitude estimate).[※] Whilst the first number *a priori* suggests negligible viscous effects, the latter implies a regime not entirely turbulent: it would be interesting to explore the effect of a viscous correction to the model. Such a correction would consist of an adjustment of the drag coëfficient — Andreotti, Forterre & Pouliquen [1] predict

$$C_\infty \mapsto C_d = \left(\sqrt{C}_\infty + k\sqrt{Re}\right)^2$$

— as well as of the addition to the force balance of a viscous term proportional to Stokes drag $3\pi\eta u_* d$.

VI · SUMMARY

From preëxisting theory, we have derived an expression for the dune migration rate which takes into account the frictional contribution of the cohesive force between the grains in the mobile layer and the rest of the bed-form. We ran forty-eight experiments, varying the diameter of the grains, the size of the dune and the velocity of the surrounding fluid. Fitting the model to the data, we found a better fit for the cohesive model than for that lacking in a cohesive term ($R^2 \approx 0.96$ against $R^2 \approx 0.85$). One parameter of our fits — the cohesive diameter d_γ — is associated with high uncertainty, and it is a matter of interest for further research to establish its exact value and properties.

[※] The conversion from v to u_* is obtained from f$^{\underline{n}}$ § (p. iv) with $a \sim 10^{-2}$, $b \sim 6 \cdot 10^{-2}$, $\varkappa \sim 10^{-1}$ and $\text{д} \sim d/30 \sim 10^{-4}$, yielding $u_* \sim 10^{-1}\, v \sim 10^{-1}$.

REFERENCES

[1] B. Andreotti, Y. Forterre & O. Pouliquen. *Granular Media. Between Fluid and Solid*. Cambridge: Cambridge University Press, 2013. ISBN: 978-1-107-03479-2.

[2] K. A. Bacik et al. "Wake-induced long-range repulsion of aqueous dunes". Submitted to *Physical Review Letters*. 2019. Pending publication.

[3] R. A. Bagnold. *An Approach to the Sediment Transport Problem from General Physics*. Report 422-1. US Government Printing Office, 1966. DOI: 10.3133/pp422I.

[4] R. A. Bagnold. "The flow of cohesionless grains in fluid". In *Philosophical Transactions of the Royal Society of London* CCXLIX (964 1956), pp. 235–297. DOI: 10.1098/rsta.1956.0020.

[5] R. A. Bagnold. "Threshold speed and grain size". In. *The Physics of Blown Sand and Desert Dunes*. London: Methuen & Co., 1941. Chap. VII.

[6] R. A. Bagnold & G. I. Taylor. "The Movement of Desert Sand". In *Proceedings of the Royal Society of London. Series A: Mathematical and Physical Sciences* CLVII (892 1936), pp. 594–620. DOI: 10.1098/rspa.1936.0218. (Visited on 15/09/2019).

[7] F. Charru, B. Andreotti & Ph. Claudin. "Sand Ripples and Dunes". In *Annual Review of Fluid Mechanics* XLV (2012), pp. 469–493. DOI: 10.1146/annurev-fluid-011212-140806.

[8] F. Charru, H. Mouilleron & O. Eiff. "Erosion and deposition of particles on a bed sheared by a viscous flow". In *Journal of Fluid Mechanics* dxix (2004), pp. 55–80. doi: 10.1017/S0022112004001028.

[9] J. M. Cimbala. *Drag on Spheres*. [Handout]. Penn State University, 2012. url: https://www.me.psu.edu/cimbala/me325web_Spring_2012/Labs/Drag/intro.pdf (visited on 16/09/2019).

[10] F. M. von Exner. "Über die Wechselwirkung zwischen Wasser und Geschiebe in Flüssen". In *Sitzungsberichte der Kaiserlichen Akademie der Wissenschaften. Mathematisch-Naturwissenschaftliche Classe* cxxxiv (2a) (1925), pp. 165–203.

[11] J. J. Fernandez Luque & R. van Beek. "Erosion and transport of bed-load sediment". In *Journal of Hydraulic Research* xiv (1976), pp. 127–144.

[12] E. M. Franklin & F. Charru. "Subaqueous barchan dunes in turbulent shear flow. Part I. Dune motion". In *Journal of Fluid Mechanics* dclxxv (2011), pp. 199–222. doi: 10.1017/S0022112011000139.

[13] Ph. Frey & M. Church. "Bedload: a granular phenomenon". In *Earth Surface Processes and Landforms* xxxvi (1) (2011), pp. 58–69. doi: 10.1002/esp.2103.

[14] D. D. Fuller. "Coefficients of friction". In. —. Columbia University. url: https://web.mit.edu/8.13/8.13c/references-fall/aip/aip-handbook-section2d.pdf (visited on 10/09/2019). [*c.* 1968].

[15] B. Gady, D. Schleef & R. Reifenberger. "Identification of electrostatic and van der Waals interaction forces between a micrometer-size sphere and a flat substrate". In *Physical Review B* liii (12) (1996). Ed. by D. Rimai & L. P. DeMejo.

[16] P. Y. Julien. *Erosion and Sedimentation*. Cambridge: Cambridge University Press, 1998.

[17] Th. Pähtz & O. Durán. "Fluid Forces or Impacts: What Governs the Entrainment of Soil Particles in Sediment Transport Mediated by a Newtonian Fluid?" In *Physical Review Fluids* ii (7) (2017). issn: 2469-990X. doi: 10.1103/PhysRevFluids.2.074303. arXiv: 1605.07306.

[18] K. Pye. "Coastal dunes". In *Progress in Physical Geography: Earth and Environment* vii (4) (1983), pp. 531–557. doi: 10.1177/030913338300700403.

[19] K. Pye & H. Tsoar. *Æolian Sand and Sand Dunes*. Berlin: Springer, 2009. isbn: 978-3-540-85909-3. doi: 10.1007/978-3-540-85910-9.

[20] A. S. Walker. *Deserts: geology and resources*. General interest publication. Washington D. C.: U. S. Geological Survey, 1996. Chap. 'Types of Dunes'. 64 pp. doi: 10.3133/7000004. url: https://pubs.usgs.gov/gip/deserts/dunes/ (visited on 15/09/2019).

CONTENTS

LIST OF FIGURES

LIST OF TABLES

Appendices

A · ADDITIONAL FIGURES

A.1 Sample plots

We include here three more sample plots: one to exemplify the three-dimensional wrap-around plot which is used to circumvent the inconvenience of a branch cut (fig. 14); and the latter two to show the level of variation we experience in the tightness of the fits to find the migration rate (figs. 15 and 16).

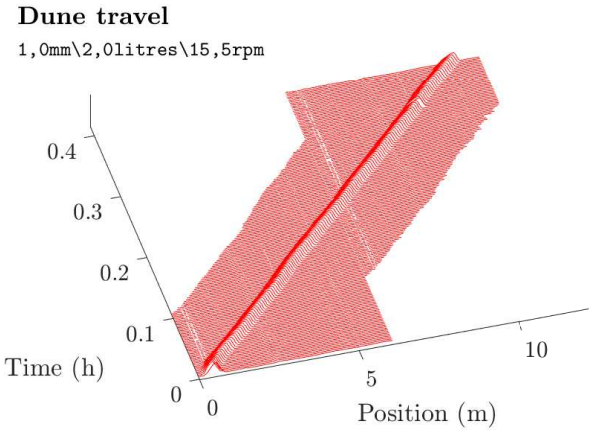

Figure 14: An example space-time diagram. *Data have been repeated then pruned to circumvent doublets due to the periodic nature of the tank.*

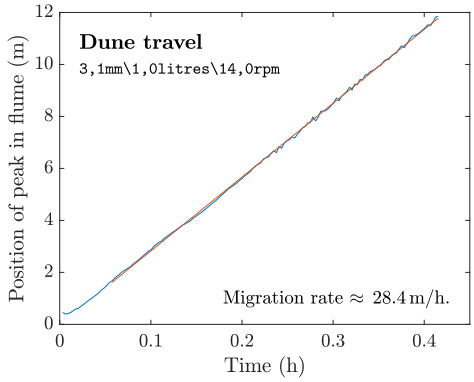

Figure 15: A particularly good run.

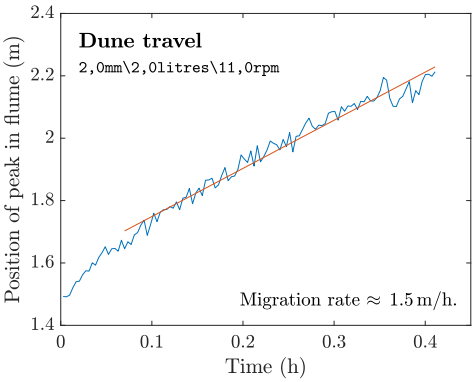

Figure 16: Wider variation in the position. *We believe this to occur with large flat dunes, where the maximum of the bed-form is influenced by differences on the order of one grain.*

A.2 Comparing v and Ω

A note on v and Ω. — Throughout the analysis, we have used our velocimetric quantity v instead of the driving rotation rate Ω, because v is expected to relate more closely to the turbulent shear velocity u_*, which features in all of the theory. It is reasonable to ask, however, how the flow in our tank relates to its rate of rotation Ω. To that end, we plot one against the other in fig. 17.

We find a relationship that is reasonably affine in the region of interest. Though it is expected that these two quantities should therefore be — within reason — interchangeable, we find the quality of our fits significantly reduced if we attempt to use Ω (*v.* fig. 20, p. xx).

B · DUNE HEIGHT

We reproduce scaled plots of the heights used in the data analysis. These are rescaled to compare

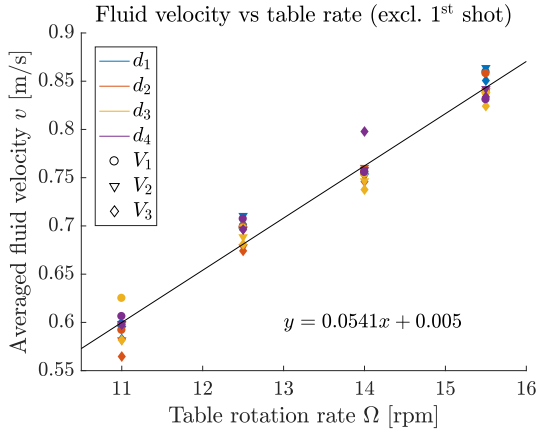

Figure 17: Response of the fluid in the tank to rotation.

dunes of different heights: for shape-invariant dunes, $V \simeq H^2$, so any variation in $H/\sqrt{V}$ betrays variation in the dunes' shape. Since our measurements for mass are of better accuracy, we use mass as an analogue for volume. The values of the mass are in table 3, with m_1, m_2 and m_3 corresponding to the three sizes of dunes we considered (V_1, V_2 and V_3). These match very closely for all grain sizes apart from d_3 (approx. 2 mm). It is not clear whether this means that those grains pack differently, or whether it was an oversight when measuring out the volume.

Looking at figs. 18 and 19, it is interesting to note that the height is not quite constant: for all but the smallest grains, the heights are ordered as V_3, V_2 then V_1. This suggests that smaller dunes may be somewhat steeper than larger ones; alternatively, it could be an artefact of varying packing fraction. The idea that dunes are not scale invariant is not alien to Franklin & Charru [12], who find an empirical fit $H \propto L - L_0$ appropriate. Figure 19 is quite interesting: it appears that the relative height is not constant but instead increasing with fluid velocity, up to a point.

d	m_1 [kg]	m_2 [kg]	m_3 [kg]
d_1	1.586	2.400	3.194
d_2	1.584	2.326	3.137
d_3	1.745	2.634	3.533
d_4	1.562	2.326	3.124

Table 3: The masses of the dunes in different runs. *All numbers are given to a precision of* ± 0.005 kg.

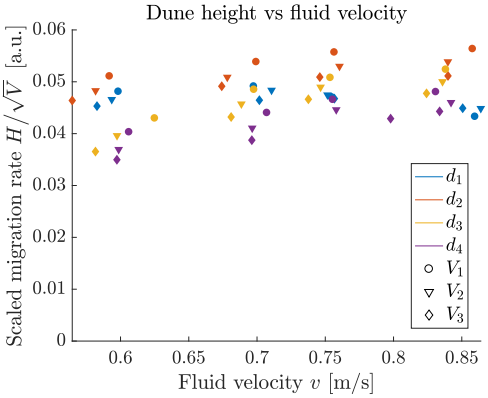

Figure 18: Scaled dune heights. *The mass m_i ($i \in [3]$) is used as an analogue for the volume V_i, for its greater accuracy (*± 0.005 kg*).*

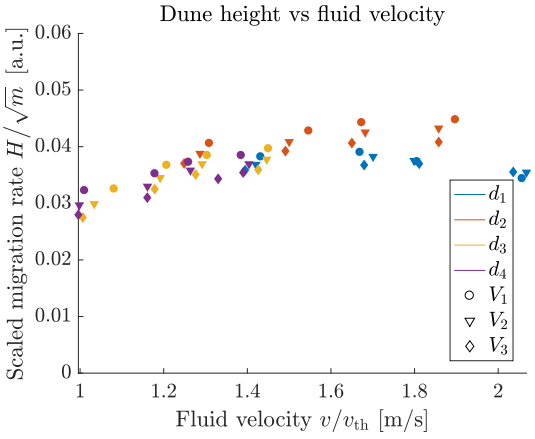

Figure 19: Scaled dune heights plotted against rescaled fluid velocity, for reference.

H		Ω_1	Ω_2	Ω_3	Ω_4
V_1	d_1	4.81	4.91	4.70	4.33
	d_2	5.11	5.38	5.57	5.63
	d_3	4.30	4.85	5.08	5.24
	d_4	4.03	4.40	4.66	4.80
V_2	d_1	5.71	5.92	5.81	5.49
	d_2	5.91	6.23	6.49	6.60
	d_3	4.85	5.60	6.00	6.13
	d_4	4.53	5.03	5.46	5.63
V_3	d_1	6.41	6.57	6.61	6.35
	d_2	6.56	6.95	7.20	7.23
	d_3	5.17	6.11	6.59	6.76
	d_4	4.94	5.48	6.07	6.26

Table 4: The dune height H for every different run. *Heights are expressed in centimetres.*

B.1 Raw dune heights

Reproduced in table 4 are the dune heights measured for every individual run.

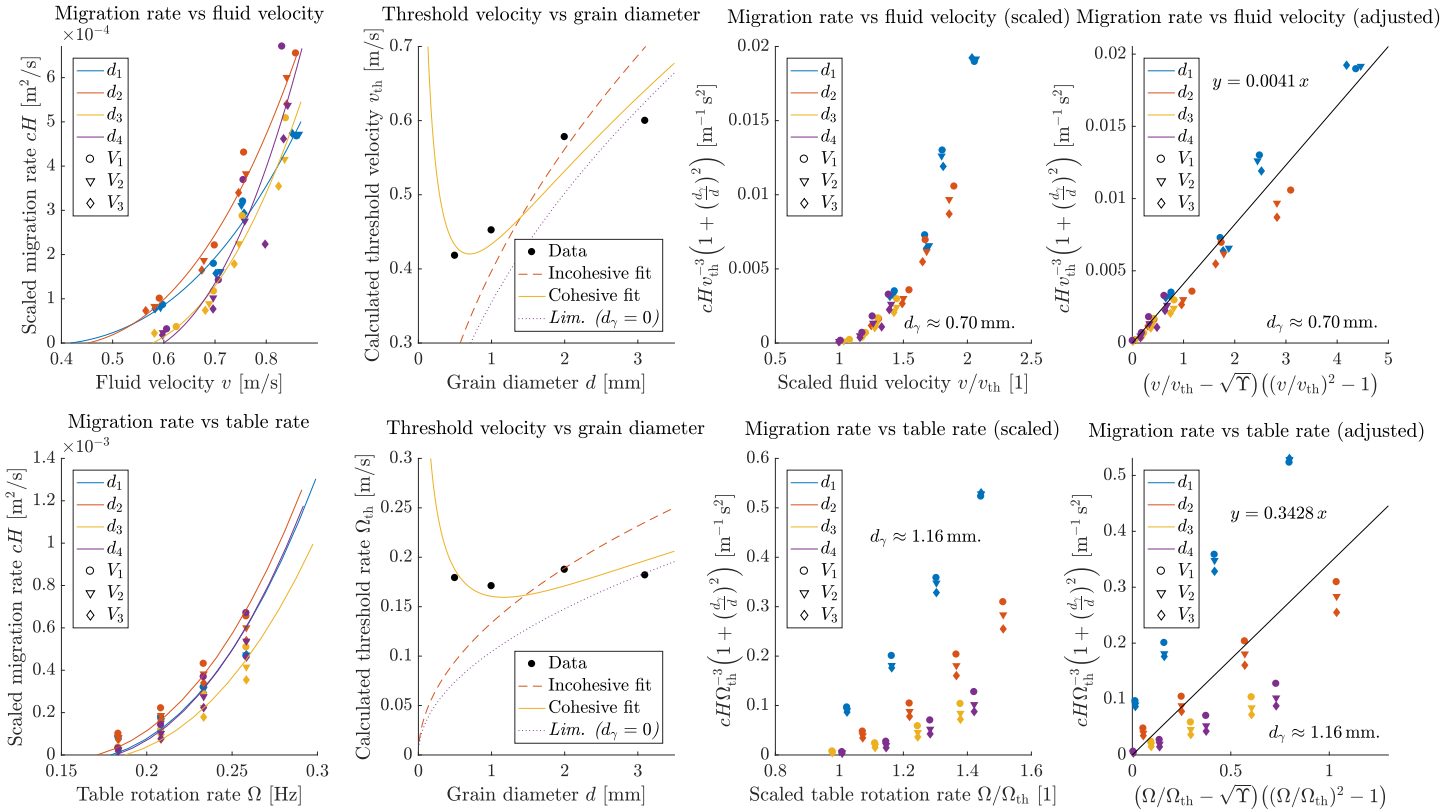

Figure 20: An extensive comparison of the plots produced using v with those produced using Ω. *Note that the plots produced with Ω give strongly unsatisfactory fits; it is not entirely clear why so large a discrepancy exists, though it may be related to inflexibility in Ω — due to the lack of independent verification — causing difficulty for the fitting routine.*